

Single-particle momentum distribution of Efimov states in noninteger dimensions

D. S. Rosa,¹ T. Frederico,¹ G. Krein,² and M. T. Yamashita²

¹*Instituto Tecnológico de Aeronáutica, DCTA, 12228-900 São José dos Campos, SP, Brazil*

²*Instituto de Física Teórica, Universidade Estadual Paulista,
Rua Dr. Bento Teobaldo Ferraz, 271-Bloco II, 01140-070 São Paulo, SP, Brazil*

We studied the single-particle momentum distribution of mass-imbalanced Efimov states embedded in noninteger dimensions. The contact parameters, which can be related to the thermodynamic properties of the gas, were calculated from the high momentum tail of the single particle densities. We studied the dependence of the contact parameters with the progressive change of the noninteger dimension, ranging from three ($D=3$) to two ($D=2$) dimensions. Within this interval, we move from the ($D=3$) regime where the Efimov discrete scale symmetry drives the physics, until close to the critical dimension, which depends on the mass imbalance, where the continuum scale symmetry takes place. We found that the two- and three-body contacts grow significantly in magnitude with the decrease of the noninteger dimension towards the critical dimension, impacting observables of resonantly interacting trapped Bose gases.

I. INTRODUCTION

More than 20 years of advances in cold-atom technologies allowed not only the experimental confirmation of Efimov states in homo [1–3] and heteronuclear atomic systems [4–6] but also lead to the burst of the rich research area of Efimov Physics. Nowadays, atomic traps give remarkable freedom to conveniently manipulate energies and geometries to study several aspects of few-body physics. Magnetic fields tuned to a Feshbach resonance [7] allow controlling the value of scattering lengths, and asymmetrical magnetic fields allow squeezing atomic clouds to create tri- [8], two- [9], and one-dimensional [10] environments.

The achievement of the universal regime, in that the scattering length tends to infinity, effectively made possible the experimental confirmation of Efimov states—weakly-bound systems originally predicted by Vitaly Efimov in 1970 when studying three identical bosons [11, 12]. This effect is characterized by the three-boson system exhibiting an infinite number of geometrically spaced energy levels (see Refs. [13–16] for reviews), and was first observed through indirect measurement of the three-body loss peaks in trapped cold atomic systems [17]. Nowadays, advanced experimental techniques allow the direct measurement of the binding energies of two- and three-body molecules in cold atomic gases [18, 19].

A myriad of developments followed since the experimental confirmation of Efimov states. One of the most notable developments is the measurements (e.g. those of Refs. [20–24]) of the Tan’s contacts [25–27], remarkable universal quantities that parameterize thermodynamic relations between macroscopic observables such as the momentum distribution, energy, and response functions of low-temperature gases interacting via short-range interactions. Tan found those universal relations by studying the tail of the two-body momentum distribution of unitary Fermi gases. For unitary Bose gases, there is one more contact parameter [28], related to the probability

of finding three atoms close together.

Since a long time, it is known the determinant role played by the spatial dimension for the presence of the Efimov effect in a three-body system—it is present in three dimensions but absent in two [29, 30]. As a consequence, in two dimensions physical properties of few- and many-boson systems scale with the two-body energies in the limit of zero-range interactions [31]. Tan’s contacts, in particular also reflect such a scaling [32]. Therefore, the sequential disappearance of the most excited bound states during a progressive change in the effective dimension of a confined resonant three-body system should also have consequences for Tan’s contacts.

An efficient way to study a dimensional crossover is to introduce a continuous dimension D and solve the three-body problem employing only the inter-atomic interactions, with the D -dependent centrifugal barrier mocking the external squeezing potential [33–37]. Although technically convenient to implement, connecting D to an experimental setup is a key issue. For three identical bosons in a deformed trap induced by an external harmonic potential, such a connection was suggested in Ref. [38] to be:

$$\frac{3(D-2)}{(3-D)(D-1)} = \left(\frac{b_{ho}}{r_{2D}} \right)^2, \quad (1.1)$$

where b_{ho} is the oscillator length and r_{2D} is the root-mean-square radius of the bound three-body system in two dimensions. A similar expression for a two-body system was suggested in Ref. [33].

Despite the advances that led to the possibility of compressing and expanding atomic clouds, creating effectively two- [9] and one-dimensional [10] setups, to the best of our knowledge, there are not yet experiments designed to study the effects of continuous deformation of the trap on Efimov physics. While awaiting such an experimental possibility, the rich physics revealed by previous theoretical studies warrants exploring this subject in connection with Tan’s contacts. Within such a perspective, we study in this work the D -dependence of

Tan's two- and three-body contact parameters in mass-imbalanced three-body systems featuring the Efimov effect. We extract the contact parameters from the single-particle momentum distributions at high momentum values. We treat the three-body problem in terms of D -dimensional hyperspherical coordinates [39] and solve the problem analytically using the Bethe-Peierls (BP) boundary conditions employing the method, we introduced in Ref. [40].

This work is organized as follows. In section II, for a system composed by two atoms A and a third one B , we review the derivation of the analytical D -dimensional Faddeev components of the mass-imbalanced three-body bound state wave function. Section III is devoted to the derivation of the momentum distribution of particle B in D -dimensions. We also discuss in this section, the high momentum regime of the single particle momentum distribution from where the two- and three-body contacts are obtained. Section IV shows quantitative results for the momentum density and relate them with the two- and three-body contacts for three-identical bosons and a mass-imbalanced system of the form ${}^6\text{Li}$ - ${}^{133}\text{Cs}_2$. The conclusions are given in Section V. Appendices A to D give details of the large momentum sub-leading contributions to the single particle momentum distribution discussed in Sec. III.

II. D -DIMENSIONAL EFIMOV STATE

In this section, we review the derivation of the D -dimensional three-body wave function of an Efimov state for a mass-imbalanced system at unitarity, according to our approach introduced in Ref. [40]. We found the solution of the energy eigenvalue equation for a three-particle system interacting with a zero-range potential by considering the Bethe-Peierls boundary condition [41] on the free energy eigenstate. This method uses the fact that the short-range region, where the interaction strongly affects the wave function, can be neglected as only the asymptotic region, parametrized by the scattering length, is the relevant one.

A. Configuration space

We consider three different particles with masses m_i , m_j , m_k , and coordinates \mathbf{x}_i , \mathbf{x}_j and \mathbf{x}_k . One can eliminate the center of mass coordinate and describe the system in terms of two relative Jacobi coordinates. The three sets of such coordinates are given by

$$\mathbf{r}_i = \mathbf{x}_j - \mathbf{x}_k \quad \text{and} \quad \boldsymbol{\rho}_i = \mathbf{x}_i - \frac{m_j \mathbf{x}_j + m_k \mathbf{x}_k}{m_j + m_k}, \quad (2.1)$$

where (i, j, k) are taken cyclically among $(1, 2, 3)$. The Faddeev decomposition of the three-body wave function allows to write it as a sum of three components. In the center of mass, it reads:

$$\Psi(\mathbf{x}_1, \mathbf{x}_2, \mathbf{x}_3) = \psi^{(1)}(\mathbf{r}_1, \boldsymbol{\rho}_1) + \psi^{(2)}(\mathbf{r}_2, \boldsymbol{\rho}_2) + \psi^{(3)}(\mathbf{r}_3, \boldsymbol{\rho}_3).$$

Each Faddeev component satisfies the free Schrödinger eigenvalue equation:

$$\left[\frac{1}{2\eta_i} \nabla_{\mathbf{r}_i}^2 + \frac{1}{2\mu_i} \nabla_{\boldsymbol{\rho}_i}^2 - E_3 \right] \psi^{(i)}(\mathbf{r}_i, \boldsymbol{\rho}_i) = 0, \quad (2.2)$$

where E_3 is the energy eigenvalue. The reduced masses are given by $\eta_i = m_j m_k / (m_j + m_k)$ and $\mu_i = m_i (m_j + m_k) / (m_i + m_j + m_k)$. For convenience, we simplify the form of the kinetic energies introducing the new coordinates $\mathbf{r}'_i = \sqrt{\eta_i} \mathbf{r}_i$ and $\boldsymbol{\rho}'_i = \sqrt{\mu_i} \boldsymbol{\rho}_i$. The three sets of primed coordinates are related to each other by the orthogonal transformations

$$\begin{aligned} \mathbf{r}'_j &= -\mathbf{r}'_k \cos \theta_i + \boldsymbol{\rho}'_k \sin \theta_i, \\ \boldsymbol{\rho}'_j &= -\mathbf{r}'_k \sin \theta_i - \boldsymbol{\rho}'_k \cos \theta_i, \end{aligned} \quad (2.3)$$

where $\tan \theta_i = [m_i M / (m_j m_k)]^{1/2}$, with $M = m_1 + m_2 + m_3$.

Considering three distinct bosons in a state with vanishing total angular momentum, one can write a reduced Faddeev component as $\chi_0^{(i)}(r'_i, \rho'_i) = (r'_i \rho'_i)^{(D-1)/2} \psi^{(i)}(r'_i, \rho'_i)$. The solution of the corresponding eigenvalue equation for $\chi_0^{(i)}$ is found by using hyperspherical coordinates to separate the variables $r'_i = R \sin \alpha_i$ and $\rho'_i = R \cos \alpha_i$, so that one can write $\chi_0^{(i)}(R, \alpha_i) = C^{(i)} F(R) G^{(i)}(\alpha_i)$, where $R^2 = r_i'^2 + \rho_i'^2$ and $\alpha_i = \arctan(r'_i / \rho'_i)$. The functions $F(R)$ and $G^{(i)}(\alpha_i)$ satisfy the following differential equations:

$$\begin{aligned} \left[-\frac{\partial^2}{\partial R^2} + \frac{s_n^2 - 1/4}{R^2} + 2\kappa_0^2 \right] \sqrt{R} F(R) &= 0, \quad (2.4) \\ \left[-\frac{\partial^2}{\partial \alpha_i^2} - s_n^2 + \frac{(D-1)(D-3)}{\sin^2 2\alpha_i} \right] G^{(i)}(\alpha_i) &= 0 \end{aligned} \quad (2.5)$$

where $-\kappa_0^2 = E_3$ and s_n is recognized as the Efimov parameter.

The definitions $z = \cos 2\alpha_i$ and $G^{(i)} = (1 - z^2)^{1/4} g^{(i)}$ turn Eq. (2.5) into the associated Legendre differential equation [42] with known analytical solutions:

$$\begin{aligned} G^{(i)}(\alpha_i) &= \sqrt{\sin 2\alpha_i} \left[P_{s_n/2-1/2}^{D/2-1}(\cos 2\alpha_i) \right. \\ &\quad \left. - \frac{2}{\pi} \tan[\pi(s_n - 1)/2] Q_{s_n/2-1/2}^{D/2-1}(\cos 2\alpha_i) \right] \end{aligned} \quad (2.6)$$

where $P_n^m(x)$ and $Q_n^m(x)$ are the associated Legendre functions. A finite value for the Faddeev component $\psi^{(i)}$ at $\rho_i = 0$ imposes that $G^{(i)}(\alpha_i = \pi/2) = 0$, since $\rho'_i = R \cos \alpha_i$.

Considering the solution of the hyperradial equation (2.4), and the hyperangular eigenfunction, Eq. (2.6), each Faddeev component of the wave function is written as [40]:

$$\begin{aligned} \psi^{(i)}(r'_i, \rho'_i) = & C^{(i)} \frac{K_{s_n} \left(\sqrt{2}\kappa_0 \sqrt{r'^2_i + \rho'^2_i} \right)}{(r'^2_i + \rho'^2_i)^{D/2-1/2}} \frac{\sqrt{\sin [2 \arctan (r'_i/\rho'_i)]}}{\left\{ \cos [\arctan (r'_i/\rho'_i)] \sin [\arctan (r'_i/\rho'_i)] \right\}^{D/2-1/2}} \\ & \times \left[P_{s_n/2-1/2}^{D/2-1} \left\{ \cos [2 \arctan (r'_i/\rho'_i)] \right\} - \frac{2}{\pi} \tan [\pi(s_n - 1)/2] Q_{s_n/2-1/2}^{D/2-1} \left\{ \cos [2 \arctan (r'_i/\rho'_i)] \right\} \right], \end{aligned} \quad (2.7)$$

where K_{s_n} is the modified Bessel function of the second kind.

The Efimov parameter s_n is obtained considering that all three pairs of particles interact resonantly. The BP boundary condition at the unitary limit [40] must be satisfied by the three-body wave function when each relative distance between two of the particles tends to zero. Taking the three cyclic permutations of $\{i, j, k\}$ one has a homogeneous linear system:

$$\frac{C^{(i)}}{2} \left[(\cot \alpha_i)^{\frac{D-1}{2}} \left(\sin 2\alpha_i \frac{\partial}{\partial \alpha_i} + D - 3 \right) G^{(i)}(\alpha_i) \right]_{\alpha_i \rightarrow 0} + (D-2) \left[\frac{C^{(j)} G^{(j)}(\theta_k)}{(\sin \theta_k \cos \theta_k)^{\frac{D-1}{2}}} + \frac{C^{(k)} G^{(k)}(\theta_j)}{(\sin \theta_j \cos \theta_j)^{\frac{D-1}{2}}} \right] = 0, \quad (2.8)$$

for $i \neq j \neq k$.

The Efimov parameter, s_n , is obtained by solving the characteristic transcendental equation of the system. When s_n is purely imaginary ($s_n \rightarrow is_0$), the effective $1/R^2$ potential in Eq. (2.4) is attractive, giving rise to the well known Landau “fall-to-center”, where the energy spectrum is unbounded from below—a behavior first found by by Thomas [43] for a neutron-deuteron nuclear system.

B. Momentum space

To obtain the single particle momentum distributions, one needs to perform the Fourier Transform (FT) of the Faddeev wave functions, Eq. (2.7). However, instead of performing the FT directly, we first obtain the spectator amplitude. The asymptotic form of the associated Legendre polynomials for $r'_i \rightarrow 0$ in the hyperangular part of the Faddeev wave function, Eq. (2.6), has to be used, which leads to:

$$\begin{aligned} \psi^{(i)}(\rho'_i, r'_i) \Big|_{r'_i \rightarrow 0} = & C^{(i)} \frac{\sqrt{2} [1 - i \cot (D\pi/2) \tanh (s_0\pi/2)]}{\Gamma (2 - D/2)} \\ & \times r'^{2-D}_i \frac{K_{is_0} (\sqrt{2}\kappa_0 \rho'_i)}{\rho'_i}, \end{aligned} \quad (2.9)$$

where $\Gamma(z)$ is the gamma function defined for all complex numbers z , except for the non-positive integers—this condition restricts the validity of our results to the interval $2 \leq D < 4$.

The spectator function, namely $B^{(i)}(\rho_i)$, can be found by taking advantage of the fact that each Faddeev component $\psi^{(i)}(\rho'_i, r'_i)$ obeys the Schrödinger’s equation for the contact interaction, written as:

$$\left[\nabla_{r'_i}^2 + \nabla_{\rho'_i}^2 - 2\kappa_0^2 \right] \psi^{(i)}(r'_i, \rho'_i) = \delta(r'_i) B^{(i)}(\rho'_i). \quad (2.10)$$

We substitute Eq. (2.9) in (2.10), which, in the limit $r'_i \rightarrow 0$, gives:

$$\begin{aligned} B^{(i)}(\rho'_i) = & C^{(i)} \frac{2^{3/2} \pi^{D/2} [1 - i \cot (D\pi/2) \tanh (s_0\pi/2)]}{\Gamma(D/2) \Gamma(2 - D/2)} \\ & \times \frac{K_{is_0} (\sqrt{2}\kappa_0 \rho'_i)}{\rho'_i}. \end{aligned} \quad (2.11)$$

Now, we take the D -dimensional FT

$$\int d^D \rho'_i \exp(-i\mathbf{q}'_i \cdot \boldsymbol{\rho}'_i) B^{(i)}(\rho'_i) = \chi^{(i)}(q'_i), \quad (2.12)$$

to write the spectator function in momentum space ($q'_i = q_i/\sqrt{\mu_i}$) as:

$$\begin{aligned} \chi^{(i)}(q'_i) = & C^{(i)} \tilde{\mathfrak{F}}_{(D,s_0)} \kappa_0^{1-D} \\ & \times H_2 \tilde{F}_1 \left(\mathcal{F}_{(D,s_0)}^*, \mathcal{F}_{(D,s_0)}, \frac{D}{2}, -\frac{q_i^2}{2\kappa_0^2} \right), \end{aligned} \quad (2.13)$$

where

$$\begin{aligned} \tilde{\mathfrak{F}}_{(D,s_0)} \equiv & i \frac{2^{D/2+1} \pi^{D-1} \Gamma[\mathcal{F}_{(D,s_0)}] \Gamma[\mathcal{F}_{(D,s_0)}^*]}{(D-2)} \\ & \times \cos \left(\frac{\pi}{2} (D - is_0) \right) \operatorname{csch} \left(\frac{\pi}{2} s_0 \right) \end{aligned} \quad (2.14)$$

and $H_2 \tilde{F}_1(a, b, c, z)$ is the regularized hypergeometrical function with $\mathcal{F}_{(D,s_0)} \equiv (D-1 + is_0)/2$.

The characteristic log-periodic behavior of the spectator functions exhibited in the Efimov region is present in the asymptotic form of the spectator functions, which is found from Eq. (2.13) at large momentum as

$$\begin{aligned} \chi_0^{(i)}(q'_i) = & C^{(i)} \tilde{\mathfrak{F}}_{(D,s_0)} 2\sqrt{\operatorname{Re}(\mathcal{G})^2 + \operatorname{Im}(\mathcal{G})^2} \\ & \times \left(\frac{q'_i}{\sqrt{2}} \right)^{1-D} \cos \left[s_0 \ln \left(\frac{q'_i}{\sqrt{2}\kappa_0^*} \right) \right], \end{aligned} \quad (2.15)$$

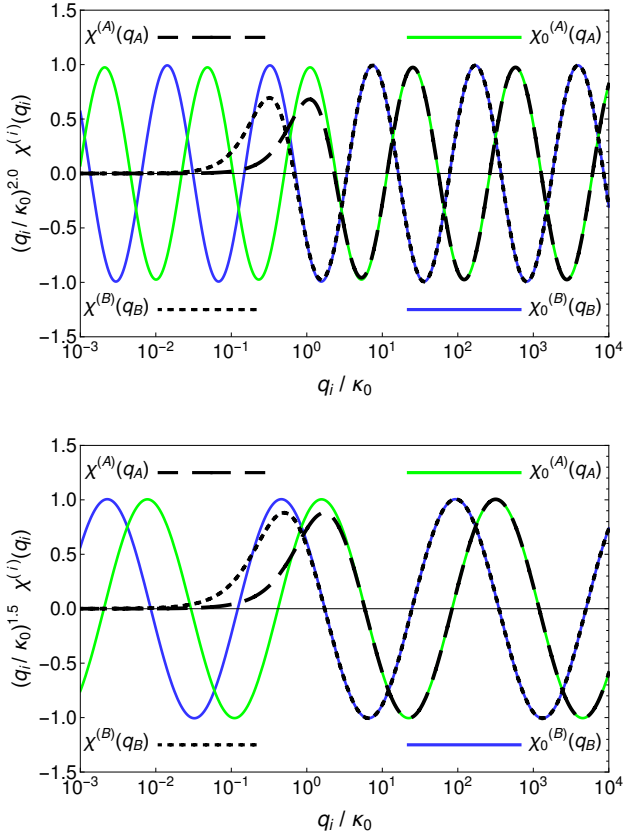


FIG. 1. Spectator functions in momentum space for the ${}^6\text{Li}-{}^{133}\text{Cs}_2$ system with finite three-body energy, $\chi^{(i)}(q_i)$ ($i = A \equiv {}^{133}\text{Cs}$ or $B \equiv {}^6\text{Li}$), computed with Eq. (2.13) for $\chi^{(A)}(q_A)$ (long-dashed line) and $\chi^{(B)}(q_B)$ (short-dashed line), compared to the zero-energy case from Eq. (2.15) for $\chi_0^{(A)}(q_A)$ (green solid line) and $\chi_0^{(B)}(q_B)$ (blue solid line). Top: three dimensions. Bottom: $D = 2.5$, which corresponds to a harmonic-trap length of $b_{ho}/r_{2D} = \sqrt{2}$.

where $\kappa_0^* \equiv \kappa_0 / \exp\{\arctan[\text{Im}(\mathcal{G})/\text{Re}(\mathcal{G})]/s_0\}$ and

$$\mathcal{G} = \frac{\Gamma(\mathcal{F}_{(D,s_0)} - \mathcal{F}_{(D,s_0)}^*)}{\Gamma(\mathcal{F}_{(D,s_0)} - D/2 - 1)\Gamma(\mathcal{F}_{(D,s_0)})}. \quad (2.16)$$

We note that the asymptotic form of the spectator function in Eq. (2.15) also corresponds to the limit of vanishing the three-body energy, with κ_0^* associated with the necessary three-body scale parameter, which is chosen to match Eq. (2.15) with the large momentum behavior of Eq. (2.13) for the finite energy spectator function. The normalization constants are solutions of Eq. (2.8), namely, the linear homogeneous system that determines the Efimov parameter.

Figure 1 shows the spectator functions, Eq. (2.13), compared to the zero energy case, Eq. 2.15 conveniently normalized to one for an AAB system with $A = {}^{133}\text{Cs}$ and $B = {}^6\text{Li}$ embedded in two different dimensions, namely $D = 3$ (top panel) and 2.5 (bottom panel). In

the low momentum region, the damping of the spectator amplitude with respect to the zero-energy case is an effect of the finite three-body binding energy. The impact of changing the dimension in which the ${}^6\text{Li}-{}^{133}\text{Cs}_2$ system is embedded is manifested mainly in the different log-periodicity of the spectator functions. The period increases to infinity as the system approaches the critical dimension, $D = 2.231$, for which the Efimov state disappears. The increasing separation of the log-periodic nodes towards the critical dimension is illustrated by comparing the top and bottom panels of Fig. 1, when the ${}^6\text{Li}-{}^{133}\text{Cs}_2$ system is forced to decrease from three to 2.5 dimensions, respectively. We reproduce analytically the numerical results obtained in Ref. [44] for $D = 3$.

III. MOMENTUM DISTRIBUTION

In this section, we compute the momentum distribution of the particle B for AAB systems at the unitary limit in D -dimensions. We recall that particle B is the one responsible for giving rise to an effective Efimov-like potential in the limit of heavy A 's, as we have shown in Ref. [36]. The momentum densities for particle B were analytically calculated for $D = 3$ in Ref. [44].

We start by defining \mathbf{k}_α ($\alpha = i, j, k$) as the momenta of each particle in the rest frame. We have that the Jacobi momenta from one particle to the center of mass of the other two and the relative momentum of the pairs are given, respectively, by

$$\mathbf{q}_i = \mu_i \left(\frac{\mathbf{k}_i}{m_i} - \frac{\mathbf{k}_j + \mathbf{k}_k}{m_j + m_k} \right) \quad \text{and} \quad \mathbf{p}_i = \eta_i \left(\frac{\mathbf{k}_j}{m_j} - \frac{\mathbf{k}_k}{m_k} \right). \quad (3.1)$$

In the following, we define the single-particle momentum distribution for particles of types A and B . The Faddeev components of the three-body wave function for a zero-range interacting system, composed of two identical particles A and a third one B , can be written using the FT of Eq. (2.10) and the spectator function given by Eq. (2.13).

We start writing the AAB bound state wave function in the basis $|\mathbf{q}_B \mathbf{p}_B\rangle$:

$$\langle \mathbf{q}_B \mathbf{p}_B | \Psi \rangle = \frac{1}{E_3 + p_B^2/2\eta_B + q_B^2/2\mu_B} \left[\chi^{(B)}(\mathbf{q}_B) + \chi^{(A)} \left(\left| \mathbf{p}_B - \frac{\mathbf{q}_B}{2} \right| \right) + \chi^{(A)} \left(\left| \mathbf{p}_B + \frac{\mathbf{q}_B}{2} \right| \right) \right], \quad (3.2)$$

and in the basis $|\mathbf{q}_A \mathbf{p}_A\rangle$:

$$\langle \mathbf{q}_A \mathbf{p}_A | \Psi \rangle = \frac{1}{E_3 + p_A^2/2\eta_A + q_A^2/2\mu_A} \left[\chi^{(A)}(\mathbf{q}_A) + \chi^{(B)} \left(\left| \mathbf{p}_A - \frac{\mathbf{q}_A}{1 + \mathcal{A}^{-1}} \right| \right) + \chi^{(A)} \left(\left| \mathbf{p}_A + \frac{\mathbf{q}_A}{1 + \mathcal{A}} \right| \right) \right]. \quad (3.3)$$

Here, we are using $m_A = 1$ in the mass ratio $\mathcal{A} = m_B/m_A$.

The momentum distributions in D -dimensions for particles A and B are given, respectively, by:

$$n_A(q_A) = \int d^D p_A |\langle \mathbf{q}_A \mathbf{p}_A | \Psi \rangle|^2, \quad (3.4)$$

and

$$n_B(q_B) = \int d^D p_B |\langle \mathbf{q}_B \mathbf{p}_B | \Psi \rangle|^2. \quad (3.5)$$

The AAB wave function can be determined, up to an overall constant, by obtaining the coefficients of the spectator functions from the solution of the homogeneous linear system (2.8). We use the following normalization condition:

$$\int d^D q_B n_B(q_B) = 1 \text{ or } \int d^D q_A n_A(q_A) = 1. \quad (3.6)$$

From Eqs. (3.2) and (3.5), we can split the momentum density into nine terms, which can be reduced to four, considering the symmetry between the two identical particles A . This simplifies the computation of the momentum density to four contributions:

$$n_B(q_B) = n_1(q_B) + n_2(q_B) + n_3(q_B) + n_4(q_B), \quad (3.7)$$

each of which is given by

$$n_1(q_B) = |\chi^{(B)}(q_B)|^2 \int d^D p_B \frac{1}{(E_3 + p_B^2 + q_B^2 \frac{\mathcal{A}+2}{4\mathcal{A}})^2}, \quad (3.8)$$

$$n_2(q_B) = 2 \int d^D p_B \frac{|\chi^{(A)}(|\mathbf{p}_B - \mathbf{q}_B/2|)|^2}{(E_3 + p_B^2 + q_B^2 \frac{\mathcal{A}+2}{4\mathcal{A}})^2}, \quad (3.9)$$

$$n_3(q_B) = 2\chi^{(B)*}(q_B) \int d^D p_B \frac{\chi^{(A)}(|\mathbf{p}_B - \mathbf{q}_B/2|)}{(E_3 + p_B^2 + q_B^2 \frac{\mathcal{A}+2}{4\mathcal{A}})^2},$$

$$+ \text{c.c.}, \quad (3.10)$$

$$n_4(q_B) = \int d^D p_B \frac{\chi^{(A)*}(|\mathbf{p}_B - \mathbf{q}_B/2|)\chi^{(A)}(|\mathbf{p}_B + \mathbf{q}_B/2|)}{(E_3 + p_B^2 + q_B^2 \frac{\mathcal{A}+2}{4\mathcal{A}})^2}$$

$$+ \text{c.c.} \quad (3.11)$$

Our task now is to evaluate the integral expressions in Eqs. (3.8)-(3.11) and extract the contacts from the large-momentum tail of the distribution densities. The contribution $n_1(q_B)$ is straightforward to calculate:

$$n_1(q_B) = \frac{|\chi^{(B)}(q_B)|^2}{q_B^{4-D}} S_D \frac{\pi}{4} \csc\left(\frac{D\pi}{2}\right) (2-D)$$

$$\times \left(\frac{\mathcal{A}+2}{4\mathcal{A}}\right)^{D/2-2}, \quad (3.12)$$

where S_D is the area of a D -dimensional sphere. The second contribution, $n_2(q_B)$, can be computed from Eq. (3.9) making the change of variables $\mathbf{p}_B - \mathbf{q}_B/2 = \mathbf{q}_A$ as:

$$n_2(q_B) = 2 \int d^D q_A \frac{|\chi^{(A)}(q_A)|^2}{(q_A^2 + \mathbf{q}_A \cdot \mathbf{q}_B + q_B^2 \frac{\mathcal{A}+1}{2\mathcal{A}})^2}. \quad (3.13)$$

In order to identify the leading order term in the large momentum region, we perform the manipulation:

$$n_2(q_B) = 2 \int d^D q_A |\chi^{(A)}(q_A)|^2$$

$$\times \left[\frac{1}{(q_A^2 + \mathbf{q}_A \cdot \mathbf{q}_B + q_B^2 \frac{\mathcal{A}+1}{2\mathcal{A}})^2} - \frac{4\mathcal{A}^2}{(\mathcal{A}+1)^2} \frac{1}{q_B^4} \right]$$

$$+ \frac{C_2}{q_B^4}, \quad (3.14)$$

where C_2 is the two-body contact, given by

$$C_2 = \frac{8\mathcal{A}^2}{(\mathcal{A}+1)^2} S_D \int_0^\infty dq_A q_A^{D-1} |\chi^{(A)}(q_A)|^2. \quad (3.15)$$

The contact C_2 can be related to the derivative w.r.t. the scattering length of the gas's mean energy (or mean free energy at nonzero temperature). It has dimension (length) $^{D-4}$ and therefore scales as $C_2 \propto \kappa_0^{4-D}$.

From the integral representations in Eqs. (3.8)-(3.11), we obtain the oscillatory and non-oscillatory contributions to each of the four components of the momentum density at large momentum (detailed calculations of the sub-leading contributions for n_1 to n_4 at large momentum can be found in Appendices A to D). The leading and sub-leading contributions in the asymptotic region are given by:

$$n_B(q_B) = \frac{C_2}{q_B^4} + \frac{C'_3}{q_B^{D+2}}$$

$$+ \frac{C_3}{q_B^{D+2}} \cos \left[2s_0 \log \left(\frac{q_B/\kappa_0^*}{(4\mu_A\mu_B)^{1/4}} \right) + \Phi \right] + \dots \quad (3.16)$$

where C'_3 brings the known non-oscillatory behavior alongside with C_2 , C_3 and Φ , which are, respectively, the amplitudes and the phase related to the log-periodic oscillatory term. The parameter C_3 is the three-body contact, closely related to the Efimov effect as it gives the amplitude of the log-periodic function of the momentum distribution.

The contact parameter C_3 and the phase Φ of the log-periodic asymptotic density, Eq. (3.16), are computed by adding Eqs. (A3), (B7), (C4) and (D4). C'_3 is obtained by adding Eqs. (A4), (B8), (C5) and (D5). Both parameters C_3 and C'_3 scale with κ_0^2 or, equivalently, the three-body bound-state energy.

IV. QUANTITATIVE RESULTS

In this section, we present the numerical results for the momentum density in noninteger dimensions computed

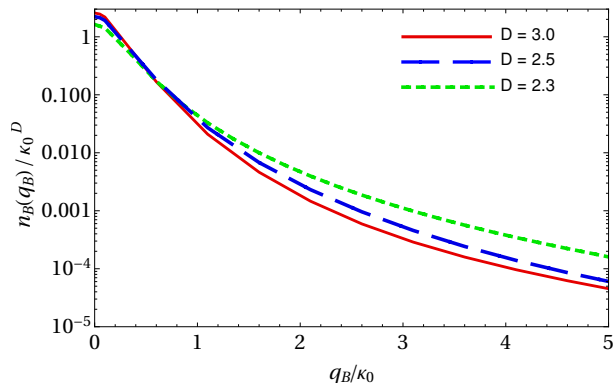


FIG. 2. Single particle momentum distribution, $n_B(q_B)$ of an ${}^6\text{Li}-{}^{133}\text{Cs}_2$ Efimov state in $D = 3$ (solid line), $D = 2.5$ (long-dashed line) and $D = 2.3$ (short-dashed line).

from Eq. (3.7) with the exact spectator function (2.13), as well as the sub-leading contributions to the density given by Eq. (3.16). We provide examples for real systems, and the contact parameters C_2 , from Eq. (3.15), C_3 and C_3' are compared with known results for three dimensions.

A. Momentum density

The normalized momentum density, $n_B(q_B)$, is shown for the low momentum region in Fig. 2, considering the ${}^6\text{Li}-{}^{133}\text{Cs}_2$ system in 3, 2.5 and 2.3 dimensions. The results for $D = 2.3$ situate close to the critical dimension where it takes place the transition between the regimes of the Efimov discrete scale symmetry to the continuum one. We observe that the squeezing of the system, by lowering the noninteger dimension, tends to emphasize the large momentum region or short-distances - this, reflects naively to a well-known result in two dimensions: any weak-attractive potential is enough to bind the system for the lowest angular momentum state.

Consequently, the large momentum region is privileged, which is also expressed by the enhancement of the momentum density and the associated two and three-body contacts. This becomes evident in the figure when one follows the decrease of the noninteger dimension by observing that density is depleted close to $q_B = 0$ and enhanced for larger values of q_B/κ_0 . What is visible in the figure is essentially the tail C_2/q_B^4 , which indicates that C_2 increases considerably from three to the critical dimension, where the Efimov effect vanishes.

In Fig. 3, we show the results for the subtracted single-particle momentum distribution ($n_B(q_B) - C_2/q_B^4$) for an Efimov state of the ${}^6\text{Li}-{}^{133}\text{Cs}_2$ system in 3 (top panel), 2.5 (middle panel) and 2.3 (bottom panel) dimensions. The results are obtained from computing Eq. (3.7) with the exact spectator function (2.13). These results are

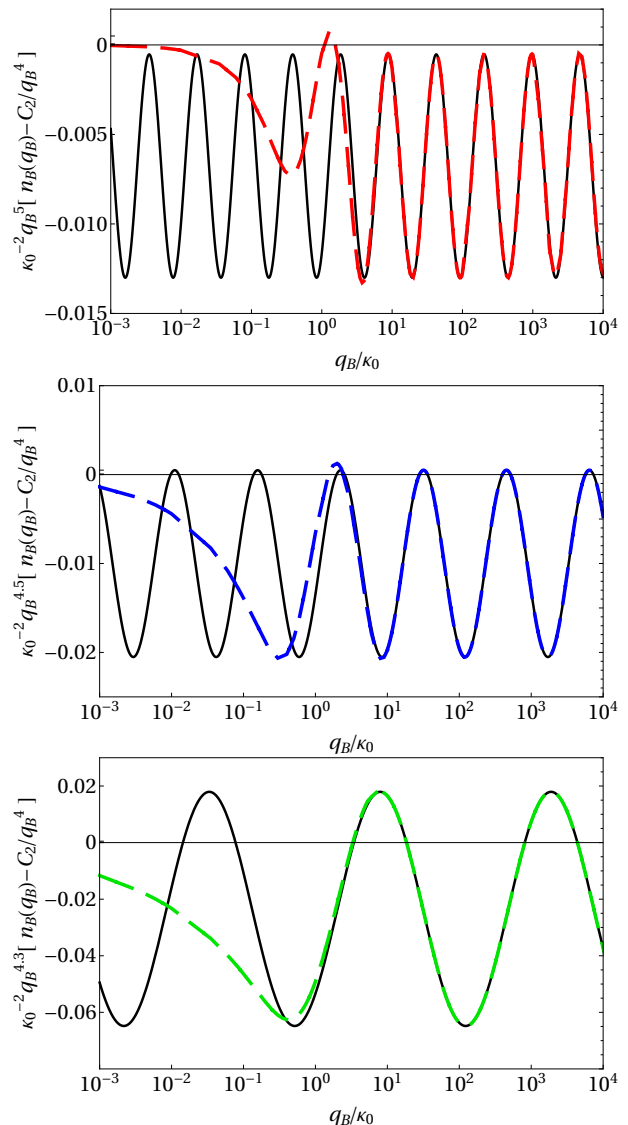


FIG. 3. Subtracted single-particle momentum distribution, $n_B(q_B) - C_2/q_B^4$, of an ${}^6\text{Li}-{}^{133}\text{Cs}_2$ Efimov state in $D = 3$ (top panel), $D = 2.5$ (middle panel) and $D = 2.3$ (bottom panel). Results obtained with regular spectator function Eq. (2.13) (dashed lines) and subtracted asymptotic formula obtained with Eq. (2.15) (solid lines).

compared with the sub-leading terms in the asymptotic expansion given in Eq. (3.16), and we found that the asymptotic region is reached quite fast and the condition $q_B \gg \kappa_0$ can be relaxed to $q_B \gtrsim \kappa_0$.

Comparing the top, middle and bottom panels, we observe the increasing separation between the nodes of the momentum distribution for 3, 2.5 and 2.3 dimensions, tending to infinity as the system approaches the critical dimension, where the Efimov effect disappears. The wavelength associated with the log-periodicity at large momentum is directly related to the value of the Efimov parameter for each noninteger dimension, such that it diverges towards the critical dimension where $s_0 \rightarrow 0$.

It is also possible to observe in Fig. 3 that the amplitude of the log-periodic oscillations raises by decreasing the dimension from three to 2.3. Such effect corresponds to the enhancement of C_3 by lowering the non-integer dimension, mimicked by strengthening the three-dimensional confinement of the system in one direction. Furthermore, we notice that the mean value reflected in $|C'_3|$ also increases. In what follows, we will further explore the dependence of the contact parameters, by changing the noninteger dimension, in two systems: ${}^6\text{Li}-{}^{133}\text{Cs}_2$ and three-identical bosons.

B. Contact parameters

We start by presenting our results for the contacts and phase for three-particle systems in three dimensions. In Table I, we compare our calculations with results from Ref. [44] for $m_B/m_A = 6/133$ and from Ref. [28] for $m_B/m_A = 1$. In Fig. 4, we illustrate the dependence of C_2 , C_3 , C'_3 and Φ for different mass ratios, ranging from heavy-heavy-light to light-light-heavy systems. In the top panel of the figure, we show results for the two and three-body parameters, C_2 , C_3 and C'_3 , considering a wide range of mass imbalanced three-body systems. In the bottom panel of Fig. 4, we show the results for the phase (Φ) of the sub-leading log-periodic term in the asymptotic form of the momentum density. We observe that C_3 , C'_3 and Φ saturate for the light-light-heavy system ($m_B/m_A \gg 1$), as well as C_2 . Furthermore, for ($m_B/m_A \gg 1$), the heavy particle B tends to be closer to the center of mass of the AAB system, increasing

TABLE I. Comparison with the contacts in three-dimensions obtained in Refs.[28, 44]. Note that the results from Ref. [28] were multiplied by a factor of $3(2\pi)^3$ to agree with the normalization from Eq. (3.6).

m_B/m_A	Contacts	Ref. [44]	Ref. [28]	our work
6/133	C_2	0.0274	-	0.0301
	C_3	-	-	0.0062
	C'_3	-	-	-0.0067
	Φ	-	-	-4.5201
1	C_2	0.0715	0.0713	0.0713
	C_3	-	0.1199	0.1199
	C'_3	0	0	0
	Φ	-	-0.8728	-0.8728

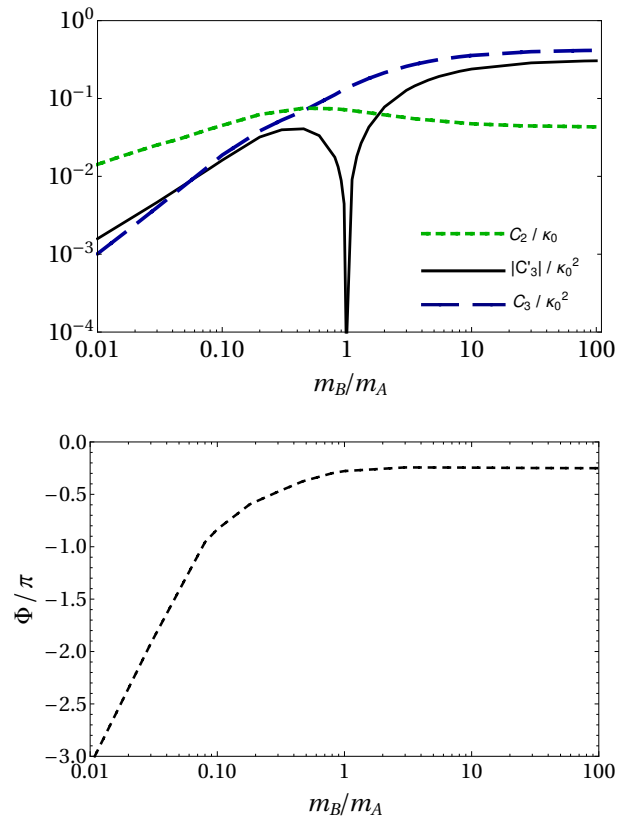


FIG. 4. Three- and two-body contact parameters (top panel) and phase (bottom panel), considering a AAB system with different mass ratios embedded in three dimensions.

the probability to find it in the large momentum region, which is reflected in the large values of the contacts, while on the other extreme for ($m_B/m_A \ll 1$), where the Efimov parameter increases and the density for the light-particle B becomes very diffuse turning less probable to find it at small distances, and consequently the contacts decrease.

We should observe that the three-body parameter C_3 is finite for any mass ratio. For three identical bosons, the contact C'_3 vanishes, as already shown in Ref. [28]. In this case, the sub-leading contribution to the momentum distribution presents a log-periodic oscillation around zero. For all the other cases where $m_A \neq m_B$, we found that C'_3 is finite, which is in agreement with the results obtained numerically in Ref. [44].

In Fig. 5, we show the dependence of the contacts and phase with the noninteger dimension for the ${}^6\text{Li}-{}^{133}\text{Cs}_2$ system from noninteger dimension 2.3 up to three. In the top panel of the figure, we observe that the contacts decrease by moving from 2.3 to three dimensions, which can be understood as the system turns to be more dilute

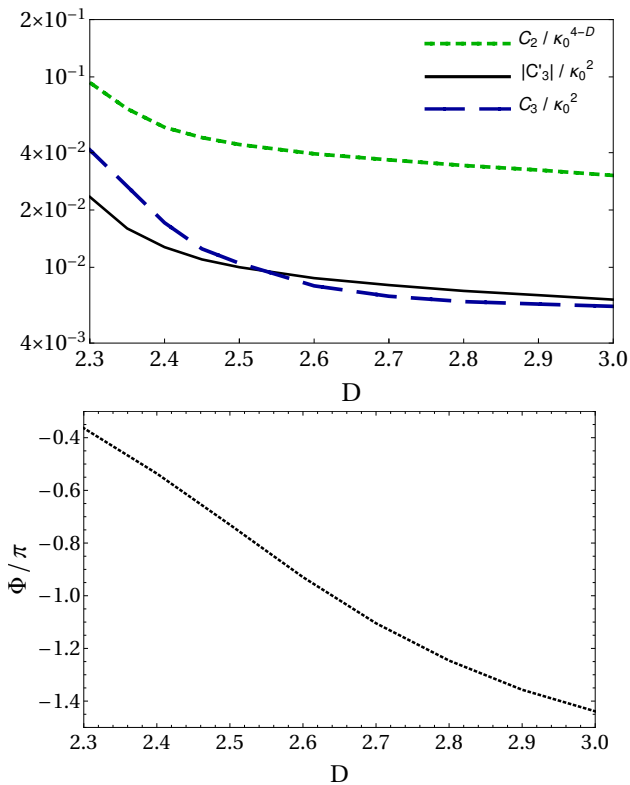


FIG. 5. Three- and two-body contact parameters and phase for the ${}^6\text{Li}-{}^{133}\text{Cs}_2$ system in noninteger dimensions from 2.3 to three. Top panel: C'_3/κ_0^2 (solid line), $|C_3|/\kappa_0^2$ (long-dashed line) and $|C_2|/\kappa_0^{4-D}$ (short-dashed line). Lower panel: phase Φ/π (dotted line).

for a fixed binding energy as the dimension increases, and in this particular case, the ${}^6\text{Li}$ is less probable to be found at short distances as one increases the dimension. Therefore, the asymptotic tail for large momentum is depleted by increasing dimension, which is reflected in the lowering of the contacts. To be complete, we present in the lower panel the phase as a function of the dimension.

Finally, in Fig. 6, we consider the case of three resonantly interacting identical bosons. We change the noninteger dimension from 3 to $D = 2.4$. In this case, the Efimov effect is present until the critical dimension of $D_c = 2.3$, which corresponds to a squeezed trap with $b_{ho}/r_{2D} = \sqrt{0.994}$. We observe in the figure, that C'_3 is always zero, while towards the critical dimension the two- and three-body contacts increase, and the phase approaches the value of -0.737 for $D = 2.4$ or squeezed trap with $b_{ho}/r_{2D} = \sqrt{1.429}$.

V. SUMMARY

In this work, we calculated the single particle momentum distribution of an Efimov mass-imbalanced state in

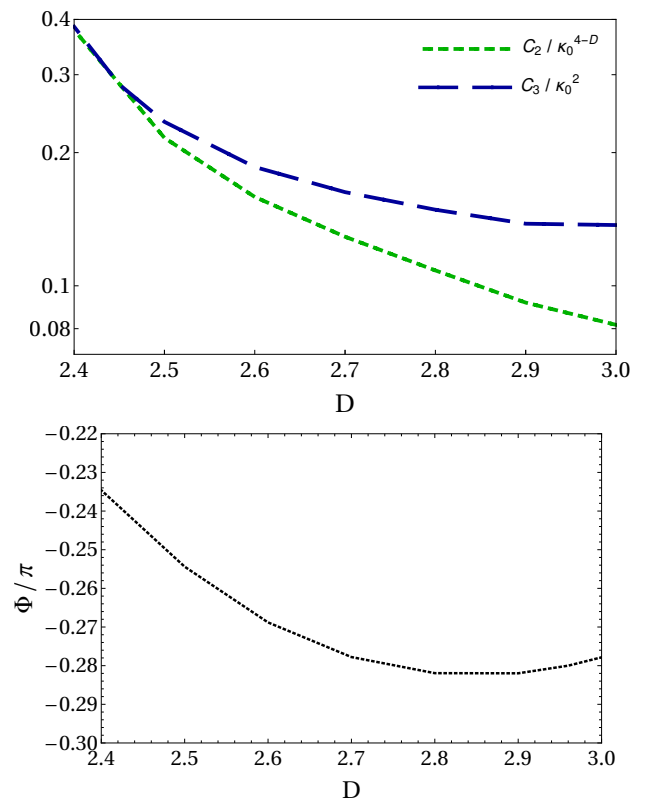


FIG. 6. Three- and two-body contact parameters and phase for three-identical bosons in noninteger dimensions. Top panel: C_3/κ_0^2 (long-dashed line) and C_2/κ_0^{4-D} (short-dashed line). Bottom panel: phase Φ/π (dotted line).

noninteger dimensions at unitarity. We used the wave function of an Efimov state with a finite three-body binding energy, obtained previously in Ref. [40] - in that reference, the three-body energy eigenstate was derived in configuration space by considering the Bethe-Peierls boundary conditions in the limit of a zero-range interaction and infinite two-body scattering length.

We studied the single particle momentum distribution in terms of the relative momentum of particle B with respect to the AA subsystem. For that, the Fourier transform of the Efimov state wave function was performed relying on the spectator functions obtained analytically by the application of the free resolvent to each Faddeev component of the wave function, following the method developed in Ref. [28]. These spectator functions depend only on the relative momentum of the spectator particle to the center of mass of the interacting pair. They have the characteristic log-periodic oscillations at large momentum, which depend on the noninteger dimension. Furthermore, due to the finite three-body binding energy, the spectator functions are finite for vanishing momentum. Their analytical form reproduces the known numerical results from the literature [44].

The task of deriving the leading and sub-leading contributions to the high momentum tail of the single particle

momentum density and the associated two- and three-body contact parameters were made possible by using the analytic form of the spectator functions in momentum space. Independently of the noninteger dimension, the leading non-oscillatory large momentum tail scales as $1/q^4$ (see Eqs. (3.14) and (3.16)) and is normalized by the two-body contact. The sub-leading term is proportional to $1/q^{D+2}$; it is composed of the sum of two contributions, a log-periodic and a non-oscillatory, each one normalized by the corresponding three-body contact as shown in Eq. (3.16).

The contact parameters were then computed by decreasing the noninteger dimension starting from 3D, where the Efimov discrete scaling drives the physics of the three-body system, until close to the critical dimension, when the transition to the continuum scale symmetry takes place. We found that the two- and three-body parameters tend to increase in magnitude close to the critical dimension, independently of the mass imbalance of the three-body system.

We explored in detail the systems formed by ${}^6\text{Li}-{}^{133}\text{Cs}_2$ and three-identical bosons. The parameter C'_3 , normalizing the sub-leading non-oscillatory term, is zero for three-identical bosons regardless of the noninteger dimension. For the ${}^6\text{Li}-{}^{133}\text{Cs}_2$ system, we found that the two- and three-body contact parameters increase close to the critical dimension where the Efimov effect disappears. Furthermore, in this case, the phase of the log-periodic term approaches -1.143 for $D = 2.4$. The expectation of the growth of the two- and three-body contact parameters with the decrease of the noninteger dimension seems natural, as one can naively infer, in this situation, the particles have the chance to stay closer to the system confined in an oblate trap.

In summary, we have explored different aspects of the momentum density of particle B for mass-imbalanced AAB systems in noninteger dimensions, which can be a useful probe into the effect of trap deformation in few-body dynamics and in the Efimov phenomenon. The hallmark of this transition from three to the critical dimension where the Efimov effect vanishes can be seen in the asymptotic momentum distribution, where we show that the contact parameters grow, and, consequently, their effects in the evolution of the many-body properties by decreasing the noninteger dimension.

ACKNOWLEDGMENTS

This work was partially supported by Fundação de Amparo à Pesquisa do Estado de São Paulo (FAPESP) [grant nos. 2017/05660-0 and 2019/07767-1 (T.F.), 2020/00560-0 (D.S.R.), and 2018/25225-9 (G.K.)], and Conselho Nacional de Desenvolvimento Científico e Tecnológico (CNPq) [grant nos. 308486/2015-3 (T.F.), 303579/2019-6 (M.T.Y.), and 309262/2019-4 (G.K.)].

Appendix A: Sub-leading contributions to $n_1(q_B)$

Eq. (3.8) can be written in spherical coordinates as

$$n_1(q_B) = |\chi^{(B)}(q_B)|^2 S_D \int_0^\infty dp_B \frac{p_B^{D-1}}{\left(E_3 + p_B^2 + \frac{q_B^2}{2\mu_B}\right)^2}, \quad (\text{A1})$$

where $S_D = 2\pi^{D/2}/\Gamma(D/2)$. Changing variables $p_B/q_B = p'_B$ and considering $q_B \gg \sqrt{2\mu_B E_3}$, allow us to write

$$\begin{aligned} n_1(q_B) &= \frac{|\chi^{(B)}(q_B)|^2}{q_B^{4-D}} S_D \int_0^\infty dp'_B \frac{p_B^{D-1}}{(p_B'^2 + 1/2\mu_B)^2} \\ &= \frac{|\chi^{(B)}(q_B)|^2}{q_B^{4-D}} S_D \frac{(2-D)\pi}{4} \csc\left(\frac{D\pi}{2}\right) (2\mu_B)^{2-D/2}. \end{aligned} \quad (\text{A2})$$

For large momentum, we use the asymptotic spectator function, Eq. (2.15), and from simple manipulations we separate the oscillatory term, namely log-periodic one:

$$\begin{aligned} n_1^{\text{osc}}(q_B) &= \frac{|C^{(B)}|^2}{q_B^{D+2}} \cos\left[2s_0 \log\left(\frac{q_B}{\sqrt{2\mu_B} \kappa_0^*}\right)\right] |\mathfrak{F}_{(D,s_0)}|^2 \\ &\times S_D \pi \left(1 - \frac{D}{2}\right) [\text{Re}(\mathcal{G})^2 + \text{Im}(\mathcal{G})^2] \\ &\times (2\mu_B)^{1+D/2} \csc\left(\frac{D\pi}{2}\right), \end{aligned} \quad (\text{A3})$$

and the non-oscillatory part as

$$\begin{aligned} n_1^{\text{nos}}(q_B) &= \frac{|C^{(B)}|^2}{q_B^{D+2}} |\mathfrak{F}_{(D,s_0)}|^2 S_D \pi \left(1 - \frac{D}{2}\right) (2\mu_B)^{1+D/2} \\ &\times [\text{Re}(\mathcal{G})^2 + \text{Im}(\mathcal{G})^2] \csc\left(\frac{D\pi}{2}\right), \end{aligned} \quad (\text{A4})$$

where \mathcal{G} is written in Eq. (2.16).

Appendix B: Sub-leading contributions to $n_2(q_B)$

Taking the large momentum limit, where $q_B \gg \sqrt{2\mu_B E_3}$, and changing variables to $\mathbf{q}_A = \mathbf{p}_B - \mathbf{q}_B/2$, Eq. (3.9) can be written as:

$$n_2(q_B) = 2 \int d^D q_A \frac{|\chi^{(A)}(q_A)|^2}{(q_A^2 + \mathbf{q}_A \cdot \mathbf{q}_B + q_B^2/2\mu_B)^2}. \quad (\text{B1})$$

In spherical coordinates we have that:

$$\begin{aligned} n_2(q_B) &= \frac{2(2\pi)^{D-3}}{q_B^4} \prod_{k=1}^{D-3} \int_0^\pi d\theta_k \sin^k \theta_k \\ &\times \int_0^\infty dq_A q_A^{D-1} |\chi^{(A)}(q_A)|^2 \int_0^\pi d\theta \sin^{D-2} \theta \\ &\times \frac{1}{[(q_A/q_B)^2 + (q_A/q_B) \cos \theta + (\mathcal{A} + 1)/2\mathcal{A}]^2}, \end{aligned} \quad (\text{B2})$$

changing variables to $q'_A = q_A/q_B$, we find that:

$$n_2(q_B) = \frac{2S_D}{q_B^{4-D}} \int_0^\infty dq'_A q_A'^{D-1} |\chi^{(A)}(q_B q'_A)|^2 \mathcal{H}(q'_A), \quad (\text{B3})$$

with

$$\begin{aligned} \mathcal{H}(y) &= \frac{4\mathcal{A}^2(D-2)}{\mathcal{A}^2(4y^4+1) + \mathcal{A}(4y^2+2) + 1} \\ &+ \frac{4\mathcal{A}^2(3-D)(2y^2\mathcal{A} + \mathcal{A} + 1)}{[2\mathcal{A}(y-1)y + \mathcal{A} + 1]^2 [2y(y+1)\mathcal{A} + \mathcal{A} + 1]} \\ &\times H_2F_1\left(1, \frac{D-1}{2}, D-1, -\frac{4\mathcal{A}y}{2(y-1)y\mathcal{A} + \mathcal{A} + 1}\right), \quad (\text{B4}) \end{aligned}$$

where $H_2F_1(a, b, c, z)$ is the hyper-geometrical function.

In order to separate the oscillatory and non-oscillatory contributions in $n_2(q_B)$ (B3), we perform the following manipulation:

$$\begin{aligned} n_2(q_B) &= \frac{2S_D}{q_B^{4-D}} \int_0^\infty dq'_A q_A'^{D-1} |\chi^{(A)}(q_B q'_A)|^2 \\ &\times \left(\mathcal{H}(q'_A) - \frac{4\mathcal{A}^2}{(\mathcal{A} + 1)^2} \right) + \frac{C_2}{q_B^4}, \quad (\text{B5}) \end{aligned}$$

where C_2 is the two-body contact parameter and was written in Eq. (3.15).

In order to derive the oscillatory part of $n_2(q_B)$ at large momentum, we introduce the asymptotic spectator function, Eq. (2.15), in the first term of Eq. (B5), i.e., $n_2(q_B) - C_2/q_B^4$. The \cos^2 from the asymptotic expression of $|\chi^{(A)}(q_B q'_A)|^2$ is algebraically manipulated in the form:

$$\begin{aligned} \cos^2 \left[s_0 \log \left(\frac{q'_A q_B}{\sqrt{2\mu_A \kappa_0^*}} \right) \right] &= \frac{1}{2} \\ &+ \frac{1}{2} \left\{ \cos \left[2s_0 \log \left(\frac{q_B}{\sqrt{2\mu_A \kappa_0^*}} \right) \right] \cos [2s_0 \log(q'_A)] \right. \\ &\left. - \sin \left[2s_0 \log \left(\frac{q_B}{\sqrt{2\mu_A \kappa_0^*}} \right) \right] \sin [2s_0 \log(q'_A)] \right\}. \quad (\text{B6}) \end{aligned}$$

we can write the oscillatory term:

$$\begin{aligned} n_2^{\text{osc}}(q_B) - \frac{C_2}{q_B^4} &= \frac{|C^{(A)}|^2}{q_B^{D+2}} \frac{2^{1+D} S_D}{\mu_A^{1-D}} [\text{Re}(\mathcal{G})^2 + \text{Im}(\mathcal{G})^2] \\ &\times |\mathfrak{F}_{(D,s_0)}|^2 \int_0^\infty dq'_A q_A'^{1-D} \left(\mathcal{H}(q'_A) - \frac{4\mathcal{A}^2}{(\mathcal{A} + 1)^2} \right) \\ &\times \left\{ \cos \left[2s_0 \log \left(\frac{q_B}{\sqrt{2\mu_A \kappa_0^*}} \right) \right] \cos [2s_0 \log(q'_A)] \right. \\ &\left. - \sin \left[2s_0 \log \left(\frac{q_B}{\sqrt{2\mu_A \kappa_0^*}} \right) \right] \sin [2s_0 \log(q'_A)] \right\}. \quad (\text{B7}) \end{aligned}$$

and the non-oscillatory one:

$$\begin{aligned} n_2^{\text{nosc}}(q_B) - \frac{C_2}{q_B^4} &= \frac{|C^{(A)}|^2}{q_B^{D+2}} \frac{2^{1+D} S_D}{\mu_A^{1-D}} [\text{Re}(\mathcal{G})^2 + \text{Im}(\mathcal{G})^2] \\ &\times |\mathfrak{F}_{(D,s_0)}|^2 \int_0^\infty dq'_A q_A'^{1-D} \left(\mathcal{H}(q'_A) - \frac{4\mathcal{A}^2}{(\mathcal{A} + 1)^2} \right). \quad (\text{B8}) \end{aligned}$$

Appendix C: Sub-leading contributions to $n_3(q_B)$

Taking $n_3(q_B)$ from Eq. (3.10) with the change of variables $\mathbf{p}_B - \mathbf{q}_B/2 = \mathbf{q}_A$ and considering the large momentum limit, namely $q_B \gg \sqrt{2\mathcal{A}E_3/(\mathcal{A} + 1)}$, we can write:

$$n_3(q_B) = \int d^D q_A \frac{2\chi^{(B)*}(q_B) \chi^{(A)}(q_A)}{(q_A^2 + \mathbf{q}_A \cdot \mathbf{q}_B + q_B^2 \frac{\mathcal{A}+1}{2\mathcal{A}})^2} + \text{c.c.} \quad (\text{C1})$$

The spectator functions are real, once again after changing variables $q_A/q_B = q'_A$ and integrating in spherical coordinates, we get that:

$$n_3(q_B) = \chi^{(B)*}(q_B) \frac{4S_D}{q_B^{4-D}} \int_0^\infty dq'_A q_A'^{D-1} \chi^{(A)}(q_B q'_A) \mathcal{H}(q'_A), \quad (\text{C2})$$

where $\mathcal{H}(q'_A)$ is given by Eq. (B4). The asymptotic form is found by using the spectator function from Eq. (2.15), leading to:

$$\begin{aligned} n_3(q_B) &= \frac{C^{(B)*} C^{(A)}}{q_B^{D+2}} 2^{D+3} S_D (\mu_B \mu_A)^{D/2-1/2} \\ &\times [\text{Re}(\mathcal{G})^2 + \text{Im}(\mathcal{G})^2] \left\{ \cos \left[s_0 \log \left(\frac{q_B}{\sqrt{2\mu_B \kappa_0^*}} \right) \right] \right. \\ &\times \cos \left[s_0 \log \left(\frac{q_B}{\sqrt{2\mu_A \kappa_0^*}} \right) \right] \int_0^\infty dq'_A \mathcal{H}(q'_A) \cos [s_0 \log(q'_A)] \\ &- \sin \left[s_0 \log \left(\frac{q_B}{\sqrt{2\mu_B \kappa_0^*}} \right) \right] \sin \left[s_0 \log \left(\frac{q_B}{\sqrt{2\mu_A \kappa_0^*}} \right) \right] \\ &\left. \times \int_0^\infty dq'_A \mathcal{H}(q'_A) \sin [s_0 \log(q'_A)] \right\}. \quad (\text{C3}) \end{aligned}$$

The algebraically manipulation of the cosines and sines in the equation above leads to identify the oscillatory term:

$$\begin{aligned} n_3^{\text{osc}}(q_B) &= \frac{C^{(B)*} C^{(A)}}{q_B^{D+2}} 2^{D+2} S_D (\mu_B \mu_A)^{D/2-1/2} \\ &\times |\mathfrak{F}_{(D,s_0)}|^2 [\text{Re}(\mathcal{G})^2 + \text{Im}(\mathcal{G})^2] \\ &\times \left\{ \cos \left[s_0 \log \left(\frac{q_B^2/\kappa_0^{*2}}{2\sqrt{\mu_A \mu_B}} \right) \right] \int_0^\infty dq'_A \mathcal{H}(q'_A) \cos [s_0 \log(q'_A)] \right. \\ &\left. - \sin \left[s_0 \log \left(\frac{q_B^2/\kappa_0^{*2}}{2\sqrt{\mu_A \mu_B}} \right) \right] \int_0^\infty dq'_A \mathcal{H}(q'_A) \sin [s_0 \log(q'_A)] \right\}, \quad (\text{C4}) \end{aligned}$$

and the non-oscillatory one as:

$$\begin{aligned} n_3^{\text{nosc}}(q_B) &= \frac{C^{(B)*} C^{(A)}}{q_B^{D+2}} 2^{D+2} S_D (\mu_B \mu_A)^{D/2-1/2} \\ &\times |\mathfrak{F}_{(D,s_0)}|^2 [\text{Re}(\mathcal{G})^2 + \text{Im}(\mathcal{G})^2] \\ &\times \left\{ \cos \left[s_0 \log \left(\sqrt{\frac{\mu_B}{\mu_A}} \right) \right] \int_0^\infty dq'_A \mathcal{H}(q'_A) \cos [s_0 \log(q'_A)] \right. \\ &\left. - \sin \left[s_0 \log \left(\sqrt{\frac{\mu_B}{\mu_A}} \right) \right] \int_0^\infty dq'_A \mathcal{H}(q'_A) \sin [s_0 \log(q'_A)] \right\}. \quad (\text{C5}) \end{aligned}$$

Appendix D: Sub-leading contributions to $n_4(q_B)$

The argument of the spectator function in Eq. (3.11) is

$$|\mathbf{p}_B \pm \frac{\mathbf{q}_B}{2}| = q_B \sqrt{\frac{p_B^2}{q_B^2} + \frac{1}{4} \pm \frac{p_B}{q_B} \cos \theta}, \quad (\text{D1})$$

then changing variables to $p_B/q_B = p'_B$ and considering the large momentum limit, one has:

$$\begin{aligned} n_4(q_B) &= \frac{1}{q_B^{4-D}} 4\pi \prod_{k=1}^{D-3} \int_0^\pi d\theta_k \sin^k(\theta_k) \\ &\times \int_0^\infty dp'_B \frac{p_B'^{D-1}}{[p_B'^2 + (\mathcal{A} + 2)/4\mathcal{A}]^2} \int_0^\pi d\theta \sin^{D-2} \theta \\ &\times \chi^{(A)*}(q_B p'_{B-}) \chi^{(A)}(q_B p'_{B+}), \end{aligned} \quad (\text{D2})$$

where $p'_{B\pm} = \sqrt{p_B'^2 + \frac{1}{4} \pm p'_B \cos \theta}$. The product of the spectator functions 2.15 allow us to write

$$\begin{aligned} \chi^{(A)*}(q_B p'_{B-}) \chi^{(A)}(q_B p'_{B+}) &= 2 [\text{Re}(\mathcal{G})^2 + \text{Im}(\mathcal{G})^2] \\ &\times |\mathfrak{F}_{(D,s_0)}|^2 \left(\frac{q_B}{\sqrt{2\mu_A}} \sqrt{p'_{B-} p'_{B+}} \right)^{2-2D} \\ &\times \left\{ \cos \left[s_0 \log \left(\frac{p'_{B+}}{p'_{B-}} \right) \right] + \cos \left[s_0 \log \left(\frac{q_B^2 p'_{B+} p'_{B-}}{2\mu_A \kappa_0^{*2}} \right) \right] \right\}. \end{aligned} \quad (\text{D3})$$

Then, the oscillatory contribution in Eq. (D2) is:

$$\begin{aligned} n_4^{\text{osc}}(q_B) &= \frac{|C^{(A)}|^2 2^{2+D} \pi^{D/2-1/2}}{q_B^{D+2} \Gamma[D/2 - 1/2]} |\mathfrak{F}_{(D,s_0)}|^2 \mu_A^{D-1} \\ &\times [\text{Re}(\mathcal{G})^2 + \text{Im}(\mathcal{G})^2] \\ &\times \int_0^\infty dp'_B \frac{p_B'^{D-1}}{[p_B'^2 + (\mathcal{A} + 2)/4\mathcal{A}]^2} \int_0^\pi d\theta \sin^{D-2} \theta \\ &\times \mathcal{W}^{1/2-D/2} \cos \left[s_0 \log \left(\frac{q_B^2}{2\mu_A \kappa_0^{*2}} \mathcal{W}^{1/2} \right) \right], \end{aligned} \quad (\text{D4})$$

where

$$\mathcal{W} = \left(p_B'^2 + \frac{1}{4} + p'_B \cos \theta \right) \left(p_B'^2 + \frac{1}{4} - p'_B \cos \theta \right).$$

The non-oscillatory contribution in Eq. (D2) can be identified as:

$$\begin{aligned} n_4^{\text{nosoc}}(q_B) &= \frac{|C^{(A)}|^2 2^{2+D} \pi^{D/2-1/2}}{q_B^{D+2} \Gamma[D/2 - 1/2]} |\mathfrak{F}_{(D,s_0)}|^2 \mu_A^{D-1} \\ &\times [\text{Re}(\mathcal{G})^2 + \text{Im}(\mathcal{G})^2] \\ &\times \int_0^\infty dp'_B \frac{p_B'^{D-1}}{[p_B'^2 + (\mathcal{A} + 2)/4\mathcal{A}]^2} \int_0^\pi d\theta \sin^{D-2} \theta \\ &\times \mathcal{W}^{1/2-D/2} \cos \left[s_0 \log \left(\sqrt{\frac{p_B'^2 + \frac{1}{4} + p'_B \cos \theta}{p_B'^2 + \frac{1}{4} - p'_B \cos \theta}} \right) \right]. \end{aligned} \quad (\text{D5})$$

-
- [1] M. Zaccanti, B. Deissler, C. D'Errico, M. Fattori, M. Jona-Lasinio, S. Müller, G. Roati, M. Inguscio and G. Modugno, *Nature* **5**, 586 (2009).
- [2] S. Knoop, F. Ferlaino, M. Mark, M. Berninger, H. Schöbel, H.-C. Nägerl and R. Grimm, *Nature Phys.* **5**, 227 (2009).
- [3] J. R. Williams, E. L. Hazlett, J. H. Huckans, R. W. Stites, Y. Zhang and K. M. O'Hara, *Phys. Rev. Lett.* **103**, 130404 (2009).
- [4] R. Pires, J. Ulmanis, S. Häfner, M. Repp, A. Arias, E. D. Kuhnle and M. Weidemüller, *Phys. Rev. Lett.* **112**, 250404 (2014).
- [5] S.-K. Tung, K. Jiménez-García, J. Johansen, C. V. Parker and C. Chin, *Phys. Rev. Lett.* **113**, 240402 (2014).
- [6] Ruth S. Bloom, Ming-Guang Hu, Tyler D. Cumby and D. S. Jin, *Phys. Rev. Lett.* **111**, 105301 (2013).
- [7] C. Chin, R. Grimm, P. Julienne and E. Tiesinga, *Rev. Mod. Phys.* **82**, 1225 (2010).
- [8] A. J. Leggett, *Rev. Mod. Phys.* **73**, 307 (2001). Erratum, *Rev. Mod. Phys.* **75**, 1083 (2003).
- [9] D. S. Petrov, M. Holzmann and G. V. Shlyapnikov, *Phys. Rev. Lett.* **84**, 2551 (2000).
- [10] M. Greiner, I. Bloch, O. Mandel, T. W. Hänsch and T. Esslinger, *Appl. Phys. B* **73**, 769 (2001).
- [11] V. Efimov, *Phys. Lett. B* **33**, 563 (1970).
- [12] V. N. Efimov, *Sov. J. Nucl. Phys.* **12**, 589 (1971).
- [13] E. Braaten and H.-W. Hammer, *Phys. Rep.* **428**, 259 (2006).
- [14] P. Naidon and S. Endo, *Rep. Prog. Phys.* **80**, 056001 (2017).
- [15] C. H. Greene, P. Giannakeas and J. Perez-Rios, *Rev. Mod. Phys.* **89**, 035006 (2017).
- [16] H. W. Hammer, S. König and U. van Kolck, *Rev. Mod. Phys.* **92**, 025004 (2020).
- [17] T. Kraemer, M. Mark, P. Waldburger, J. G. Danzl, C. Chin, B. Engeser, A. D. Lange, K. Pilch, A. Jaakkola, H.-C. Nägerl, and R. Grimm, *Nature* **440**, 315 (2006).
- [18] R. Fletcher, A. Gaunt, N. Navon, R. Smith and Z. Hadzibabic, *Phys. Rev. Lett.* **111**, 125303 (2013).
- [19] S. Musolino, H. Kurkjian, M. Van Regemortel, M. Wouters, S. Kokkelmans and V. Colussi, *Phys. Rev. Lett.* **128**, 020401 (2022).
- [20] E. Kuhnle, H. Hu, X.-J. Liu, P. Dyke, M. Mark, P. Drummond, P. Hannaford and C. Vale, *Phys. Rev. Lett.* **105**, 070402 (2010).
- [21] P. Makotyn, C. Klauss, D. Goldberger, E. Cornell and D. Jin, *Nature Phys* **10**, 116 (2014).
- [22] R. Fletcher, R. Lopes, N. Navon, R. Smith, M. Zwierlein, Z. Hadzibabic, *Science* **355**, 377 (2017).
- [23] Z. Z. Yan, Y. Ni, C. Robens, M. W. Zwierlein, *Science* **368**, 190 (2020).

- [24] Y.-Q. Zou, B. Bakkali-Hassani, C. Maury, É Le Cerf, S. Nascimbene, J. Dalibard and J. Beugnon, *Nature Communications* **12**, 760 (2021).
- [25] S. Tan, *Ann. Phys. (N.Y.)* **323**, 2952 (2008).
- [26] S. Tan, *Ann. Phys. (N.Y.)* **323**, 2971 (2008).
- [27] S. Tan, *Ann. Phys. (N.Y.)* **323**, 2987 (2008).
- [28] Y. Castin and F. Werner, *Phys. Rev. A* **83**, 063614 (2011).
- [29] T. K. Lim and P. A. Maurone, *Phys. Rev. B* **22**, 1467 (1980).
- [30] T. K. Lim and B. Shimer, *Z. Physik A* **297**, 185 (1980).
- [31] S. K. Adhikari, A. Delfino, T. Frederico, I. D. Goldman and L. Tomio *Phys. Rev. A* **37**, 3666 (1988).
- [32] F. F. Bellotti and M. T. Yamashita, *Few-Body Syst.* **56**, 905–913 (2015).
- [33] E. Garrido and A. S. Jensen and R. Álvarez-Rodríguez, *Phys. Lett. A* **383**, 2021 (2019).
- [34] D. S. Rosa, T. Frederico, G. Krein and M. T. Yamashita, *Phys. Rev. A* **97**, 050701(R) (2018). *Erratum*, *Phys. Rev. A* **104**, 029901 (2021).
- [35] R. M. Francisco, D. S. Rosa and T. Frederico, *Phys. Rev. A* **106**, 063305 (2022).
- [36] D. S. Rosa, T. Frederico, G. Krein and M. T. Yamashita, *J. Phys. B At. Mol. Opt. Phys.* **52**, 025101 (2019).
- [37] E. Garrido and A. S. Jensen, *Phys. Lett. A* **385**, 126982 (2021).
- [38] E. Garrido and A. S. Jensen, *Phys. Rev. Res.* **2**, 033261 (2020).
- [39] E. Nielsen, D. V. Fedorov, A. S. Jensen and E. Garrido, *Phys. Rep.* **347**, 373 (2001).
- [40] D. S. Rosa, T. Frederico, G. Krein and M. T. Yamashita, *Phys. Rev. A* **106**, 023311 (2022).
- [41] H. Bethe and R. Peierls, *Proc. R. Soc. A* **148**, 146 (1935).
- [42] W. Magnus, F. Oberhettinger and R. P. Soni, *Formulas and Theorems for the Special Functions of Mathematical Physics* (Springer, New York, 1966).
- [43] L. H. Thomas, *Phys. Rev.* **47**, 903 (1935).
- [44] M. T. Yamashita, F. F. Bellotti, T. Frederico, D. V. Fedorov, A. S. Jensen and N. T. Zinner, *Phys. Rev. A* **87**, 062702 (2013).